Atmos. Chem. Phys., 24, 14191–14208, 2024
https://doi.org/10.5194/acp-24-14191-2024

Atmospheric Chemistry and Physics
Open Access
EGU

Measurement report: Surface exchange fluxes of HONO during the growth process of paddy fields in the Huaihe River Basin, China

Fanhao Meng[1,3,★], Baobin Han[1,2,★], Min Qin[1], Wu Fang[1,8], Ke Tang[4], Dou Shao[1,2], Zhitang Liao[1,2], Jun Duan[1], Yan Feng[5,6], Yong Huang[5,6], Ting Ni[5,6], and Pinhua Xie[1,2,7,8]

[1]Key Laboratory of Environmental Optics and Technology, Anhui Institute of Optics and Fine Mechanics, Hefei Institutes of Physical Science, Chinese Academy of Sciences, Hefei, 230031, China
[2]University of Science and Technology of China, Hefei, 230026, China
[3]State Key Laboratory of Pulsed Power Laser Technology, National University of Defense Technology, Hefei, 230037, China
[4]School of Electrical and Photoelectronic Engineering, West Anhui University, Lu'an, 237012, China
[5]Anhui Institute of Meteorological Sciences, Anhui Province Key Laboratory of Atmospheric Science and Satellite Remote Sensing, Hefei, 230031, China
[6]Shouxian National Climatology Observatory, Huaihe River Basin Typical Farm Eco-meteorological Experiment Field of CMA, Huainan, 232200, China
[7]CAS Center for Excellence in Regional Atmospheric Environment, Institute of Urban Environment, Chinese Academy of Sciences, Xiamen, 361021, China
[8]Institute of Environment, Hefei Comprehensive National Science Center, Hefei, 230031, China
★These authors contributed equally to this work.

Correspondence: Min Qin (mqin@aiofm.ac.cn)

Received: 9 July 2024 – Discussion started: 26 July 2024
Revised: 30 October 2024 – Accepted: 31 October 2024 – Published: 20 December 2024

Abstract. Significant amounts of nitrous acid (HONO) released from soil affect the chemistry of the troposphere, thereby serving as a major precursor to hydroxyl radicals. However, the scarcity of in situ data on soil–atmosphere HONO exchange flux has constrained the understanding of emission mechanisms and the budget of reactive nitrogen. Herein, we performed measurements of HONO and NO_x fluxes over paddy fields in the Huaihe River Basin. The entire experiment involved various agricultural-management activities, including rotary tillage, flood irrigation, fertilization, paddy cultivation and growth, and top dressing. HONO and NO exhibited more upward fluxes, whereas NO_2 was deposited on the ground, with average hourly fluxes of 0.07 ± 0.22, 0.19 ± 0.53, and -0.42 ± 0.44 nmol m^{-2} s^{-1}, respectively. Continuous peaks in HONO and NO fluxes were observed during the rotary tillage period, and they exhibited a significant correlation ($R = 0.77$). Moreover, a significant correlation ($R = 0.60$) between HONO flux and the product of $J(NO_2) \times NO_2$ was observed during the daytime. The results indicate that both biological emissions from soil and light-driven NO_2 conversion are likely active, collectively influencing the diurnal pattern of HONO flux. A source analysis revealed that the unknown HONO source ($P_{unknown}$) exhibited a diurnal pattern with higher daytime and lower nighttime values. Sensitivity tests demonstrated that photo-enhanced NO_2 conversion on the ground could adequately explain $P_{unknown}$, while nocturnal HONO production derived from soil emission fluxes (ranging from 0.32 to 0.79 ppbv h^{-1}) could sufficiently elucidate nighttime $P_{unknown}$ values. Our study emphasized the variability in HONO fluxes across various agricultural-management activities, as well as the importance of heterogeneous NO_2 conversion on ground surfaces and soil emissions in HONO production.

1 Introduction

Nitrous acid (HONO) and nitrogen oxides ($NO_x = NO + NO_2$) are key components of cycles of reactive nitrogen (Nr) and significantly influence the atmospheric oxidation capacity through the hydroxyl radical (OH) and ozone (O_3) atmospheric cycles (Kratz et al., 2022; Monks et al., 2009; Weber et al., 2015). The photolysis of HONO contributes to 20 %–90 % of the OH budget, not only serving as an important source of OH in the early morning but also playing a significant role throughout the entire day (Elshorbany et al., 2009; Kim et al., 2014; Kleffmann et al., 2005; Nan et al., 2017; Xue et al., 2020). Despite the significance of HONO in atmospheric chemistry, the formation mechanism of HONO, especially that occurring during the daytime, is still not well understood. Unexpectedly large discrepancies have been found between HONO measurements and predicted values from known mechanisms, implying the existence of sources of HONO that have not yet been identified (Lee et al., 2016; Liu et al., 2019b; Sörgel et al., 2011; Su et al., 2011; Tang et al., 2015). Several potential mechanisms have been proposed to explain atmospheric HONO levels, including direct emissions from combustion processes (Nakashima and Kajii, 2017; Nie et al., 2015); the chemical equilibrium between soil nitrite (NO_2^-) and hydrogen ions (Su et al., 2011); photosensitized reactions of NO_2 on organic substances (George et al., 2005), humic acids (Han et al., 2016; Stemmler et al., 2006), soot (Monge et al., 2010), minerals (Ndour et al., 2008), urban grime (J. Liu et al., 2019), plant leaves (Marion et al., 2021), etc.; the photolysis of adsorbed nitrates/nitric acid (Ye et al., 2017; Zhou et al., 2003; Zhou et al., 2011) and ortho-nitrophenols (Bejan et al., 2006; Guo and Li, 2022); direct emissions from ammonia-oxidizing bacteria and other microorganisms (Oswald et al., 2013; Scharko et al., 2015); the desorption of adsorbed HONO from the surface by means of acid displacement processes (Vandenboer et al., 2013, 2014, 2015); and chemical reactions of hydroxylamine on the surface of soil particles (Ermel et al., 2018). Furthermore, the NH_3-promoted heterogeneous reaction of NO_2 has recently been proposed based on laboratory and field studies (Ge et al., 2019; Li et al., 2018; Xu et al., 2019); however, this mechanism and its atmospheric influences require further investigation.

Flux measurement has long been considered a useful tool for quantifying ground-level sources of HONO, providing direct insights into the production and loss processes at the surface. In recent years, micrometeorological methods, such as relaxed eddy accumulation (REA) and the aerodynamic gradient (AG) method, have been developed and applied in HONO flux research, with field observations primarily conducted in Europe and North America. Using the REA method, Ren et al. (2011), von der Heyden et al. (2022), and Zhou et al. (2011) measured HONO fluxes in various environments, such as agricultural fields, forests, and grasslands. These studies revealed that HONO fluxes are primarily driven by photosensitized NO_2 reduction and the photolysis of adsorbed HNO_3. Laufs et al. (2017), Meng et al. (2022), and Sörgel et al. (2015) performed measurements utilizing the AG method over bare soil, corn canopies, forest canopies, and wheat canopies, obtaining similar conclusions. Nevertheless, the chamber method provides greater flexibility and is suitable for multipoint observations within agricultural fields. Tang et al. (2020) and Xue et al. (2019) investigated HONO emissions from agricultural soil in the Huaihe River Basin and the North China Plain (NCP) by employing the open-top dynamic chamber method, confirming that agricultural soil emissions are an important source of atmospheric HONO. However, the limited number of available HONO flux studies indicates that there may be different potential HONO precursors, demonstrating the necessity for more HONO flux measurements to explore potential HONO formation pathways. Moreover, most flux measurements are typically conducted over the short term (less than 1 month) and cannot cover the entire growing season of crops. Research on HONO fluxes in agriculture has primarily focused on wheat–maize rotations and the effects of fertilization. Paddy fields, which cultivate a major crop in southern China under unique growth conditions, have received little attention, resulting in limited understanding of the Nr budget in paddy field ecosystems.

Croplands, which cover 50 % of global habitable areas (FAO, 2022), play a crucial role in the global nitrogen budget. The application of nitrogen fertilizers has been instrumental in boosting food production. Nevertheless, the overuse of fertilizers has also resulted in soil degradation, declining air quality, and adverse effects on human health. Simultaneously, the extensive application of synthetic nitrogen fertilizers on cropland, coupled with the fertilizers' low nitrogen use efficiency (< 50 % on average) (Mueller et al., 2017; Zhang et al., 2015), has led to the release of excess Nr from soil through microbial processes. Among these processes, NO_x mediates the production and destruction of O_3, influences the formation of the OH radical, and can be oxidized to nitric acid and nitrate, thereby increasing both the wet and dry deposition of nitrogen in ecosystems (Pilegaard, 2013). Notably, the positive effect of nitrogen fertilizers on HONO emissions has been consistently verified (Wang et al., 2021). Xue et al. (2019) reported an extraordinarily high HONO flux of 1515 ng N m^{-2} s^{-1} under excessive fertilization conditions, which greatly exceeded the emissions from unfertilized farmland and even surpassed laboratory results. This underscores the significant potential for Nr emissions originating from agricultural soil. Therefore, it is imperative to comprehend the fluxes within agricultural ecosystems to elucidate the mechanisms of Nr production and loss. The lack of field data on HONO fluxes in paddy fields, coupled with the am-

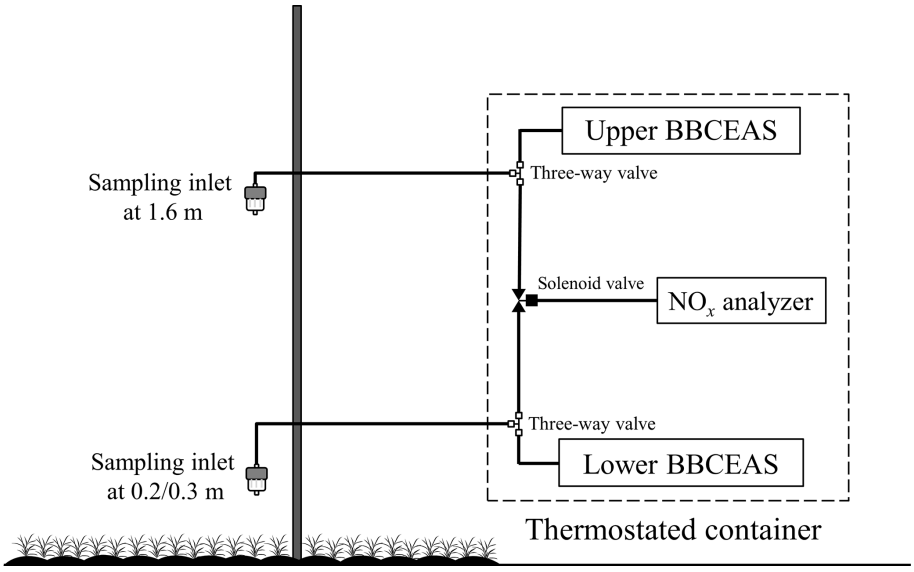

Figure 1. The aerodynamic gradient measurement setup for the determination of HONO, NO, and NO_2 fluxes. BBCEAS: broadband cavity-enhanced absorption spectrometer.

biguous impacts of agricultural-management activities, hinders our understanding of soil–atmosphere exchange mechanisms. Laboratory studies have also demonstrated HONO and NO emissions at high levels of water content (Wang et al., 2021; Wu et al., 2019), and anaerobic denitrification in oxygen-limited environments can be an important source of HONO (Bhattarai et al., 2021; Wang et al., 2021; Wu et al., 2019). This highlights the necessity of further investigating the effects of flooded paddy fields and agricultural practices on soil HONO emissions.

In this study, soil–atmosphere exchange processes in paddy fields located in the Huaihe River Basin were investigated using the AG method in conjunction with a broadband cavity-enhanced absorption spectrometer (BBCEAS) system and an NO_x analyzer. Variations in HONO and NO_x levels and fluxes were evaluated across various agricultural-management processes from June to July, corresponding to the paddy growing season. Additionally, particular focus was placed on investigating the sources of HONO during the rotary tillage period and their contribution to the atmospheric oxidizing capacity.

2 Materials and methods

2.1 Measurement site

The field campaign was conducted at the Shouxian National Climatology Observatory (32°25′ N, 116°47′ E; 25 m above sea level), located 9 km south of Shouxian, Anhui (Fig. S1 in the Supplement). This location represents a typical rice–wheat rotation ecosystem in the Huang–Huai agroecological region, which serves as the primary grain production area in China, contributing to 18 % of the nation's total grain production. Additionally, it is responsible for 76.3 % of the country's total nitrogen fertilizer application (Cao et al., 2019). The site covers a 17 ha field and is dedicated to the cultivation of rice–wheat rotations. It serves as an experimental site for studying surface–atmosphere exchange. The site is situated amidst other agricultural fields, with a low-traffic road to the north (250 m). The region has a prevailing subtropical monsoon climate, characterized by distinct seasons, with high temperatures and rainfall occurring in the same season. The average annual temperature is 14.8 °C, and the average annual precipitation amount is 905 mm.

2.2 Experimental design

The flux measurements were conducted from 1 June to 14 July 2021, immediately following the winter wheat harvest on 31 May 2021. The tillage process took place over 11 d, from 2 to 13 June, followed by periods of flood irrigation and fertilization with a compound fertilizer ($N–P_2O_5–K_2O$ (15 %–15 %–15 %)), applied at a rate of 67.5 kg N ha^{-1}, before 22 June 2021. Consequently, the surface was a mixture of bare soil and sparse winter wheat residues before irrigation took place (09:00 LT on 13 June; hereafter, all times are given in local time), while the soil became waterlogged after flood irrigation. The paddy seedlings were transplanted on 26 and 27 June at a density of 1.8×10^5 plants ha^{-1} and grew from 0.14 m to approximately 0.22 m during the campaign. Additionally, irrigation was employed following the paddy transplantation to mitigate water deficiency during the growth phase, thereby preventing the potential mortality of paddy seedlings. The 46 % N urea solution (69 kg N ha^{-1}) was applied as a top dressing on 10 July.

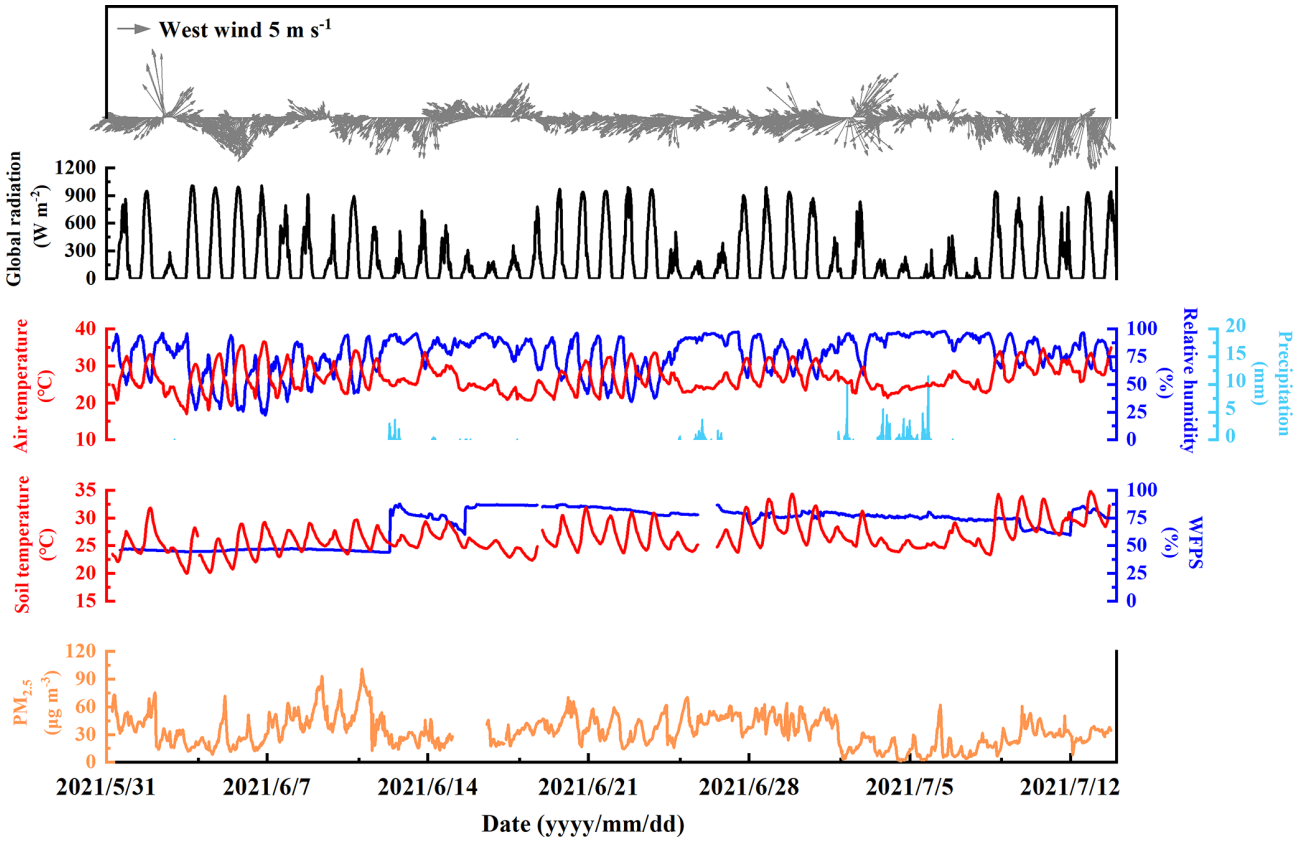

Figure 2. Temporal variations in meteorological parameters (wind speed, wind direction, air temperature, relative humidity, and precipitation), soil temperature, water-filled pore space (WFPS), and $PM_{2.5}$ measured from 1 June to 14 July 2021.

Concentrations of HONO and NO_2 in the ambient air were measured using a homemade BBCEAS instrument with a time resolution of 1 min and detection limits of 54 pptv (2σ) for HONO and 98 pptv (2σ) for NO_2. The measurement uncertainties were 8.7 % for HONO and 8.1 % for NO_2. Further details regarding the BBCEAS, such as its principle, instrument parameters, and quality control, are described in detail elsewhere (Duan et al., 2018; Tang et al., 2019). NO was measured using a custom-built chemiluminescence instrument (Model 42i-TL, Thermo Fisher Scientific, USA), and O_3 was measured using Model 49i (Thermo Fisher Scientific), with detection limits of 50 pptv for NO and 500 pptv for O_3. Measurements of soil temperature and moisture, as well as meteorological and micrometeorological parameters, are presented in Sect. S1 in the Supplement.

Trace gas profiles of HONO, NO, and NO_2 were obtained using inlets positioned at heights of 0.2 and 1.6 m, which were adjusted to 0.3 and 1.6 m, respectively, on 27 June to accommodate the canopy height, ensuring they consistently exceeded the canopy height throughout the campaign (Fig. 1). Two BBCEAS instruments were used to measure HONO and NO_2 at different heights. They were intercompared several times throughout the campaign and exhibited excellent agreement ($R^2 = 0.989$ for HONO and $R^2 = 0.998$ for NO_2), with slopes close to 1 (Fig. S2). An NO_x analyzer for NO measurements was connected to a Teflon solenoid valve to enable sequential measurements at two different heights. All instruments were placed in a thermostated container controlled by an air conditioner, with external sampling inlets affixed to a small mast. The sampling inlets were oriented away from the mast and toward the prevailing wind direction to minimize turbulence disruption. To prevent photolysis and the condensation of water vapor, the perfluoroalkoxy (PFA) inlet lines (7.5 m in length with a 6 mm external diameter) were shielded from radiation and slightly heated using heating tape, with the heating temperature set to about 30 °C.

2.3 Aerodynamic gradient fluxes of HONO, NO, and NO_2

The HONO, NO, and NO_2 fluxes were calculated using the AG method at time intervals of 30 min, as elaborated upon in previous studies (Laufs et al., 2017; Meng et al., 2022; Stella et al., 2012) and briefly introduced here. The flux (F_χ) of trace gas is calculated from the friction velocity (u_*) and the mixing-ratio scaling parameter (χ_*) as follows:

$$F_\chi = -u_* \chi_*, \quad (1)$$

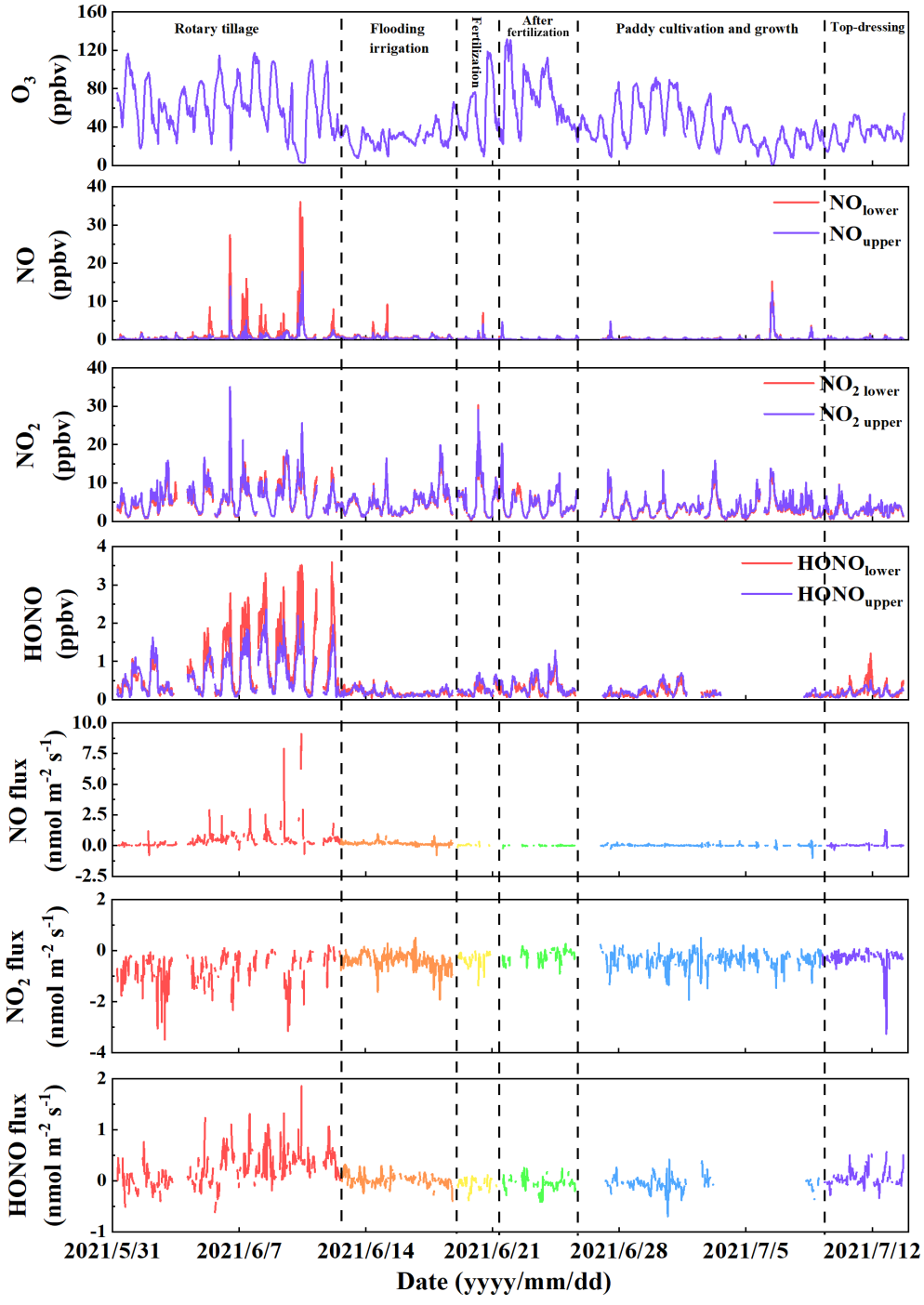

Figure 3. Time series of O_3, NO, and NO_2, as well as those of the fluxes of HONO, NO, and NO_2, were determined using the aerodynamic gradient method. The mixing ratios of HONO, NO, NO_2 (0.2–0.3 m for the lower level and 1.6 m for the upper level), and O_3 were measured above a crop rotation field and averaged over 30 min intervals. Periods of agricultural-management activities (rotary tillage, flood irrigation, fertilization, after fertilization, paddy cultivation and growth, and top dressing) are indicated at the top of the graph.

where u_* is calculated from eddy covariance measurements and χ_* is defined using the stability-corrected gradient of the scalar mixing ratio (χ) and height (z) as

$$\chi_* = \kappa \cdot \frac{\partial \chi}{\partial \left[\ln(z-d) - \Psi_H\left(\frac{z-d}{L}\right)\right]}. \quad (2)$$

Table 1. Statistical summary of HONO, NO, and NO_2 concentrations, as well as HONO flux, NO flux, and NO_2 flux, across various agricultural activities spanning the period from 1 June to 14 July 2021.

Agricultural activities		HONO (ppbv)		NO (ppbv)		NO_2 (ppbv)		HONO flux	NO flux	NO_2 flux
		0.2–0.3 m	1.6 m	0.2–0.3 m	1.6 m	0.2–0.3 m	1.6 m	(nmol m^{-2} s^{-1})	(nmol m^{-2} s^{-1})	(nmol m^{-2} s^{-1})
Rotary tillage	Ave	0.99	0.69	1.88	0.87	6.26	6.56	0.23	0.47	−0.72
	Min	0.08	0.07	0.07	0.06	0.70	0.90	−0.62	−0.78	−3.50
	Max	3.60	2.36	36.02	17.80	22.24	35.03	1.86	9.12	0.29
Flood irrigation	Ave	0.19	0.18	0.66	0.46	4.62	4.91	0.02	0.18	−0.40
	Min	0.04	0.06	0.13	0.08	1.11	1.11	−0.40	−0.78	−1.93
	Max	0.52	0.44	9.22	2.12	17.31	19.92	0.32	1.18	0.50
Fertilization	Ave	0.24	0.31	0.33	0.28	5.81	6.15	−0.06	0.03	−0.34
	Min	0.08	0.07	0.06	0.05	0.39	0.64	−0.38	−0.13	−1.37
	Max	0.61	0.71	7.02	4.14	30.30	29.07	0.11	0.31	0.07
After fertilization	Ave	0.30	0.36	0.26	0.26	4.58	4.49	−0.05	0.001	−0.19
	Min	0.06	0.05	0.05	0.06	0.69	0.88	−0.41	−0.23	−1.17
	Max	1.05	1.29	4.09	4.61	19.25	20.32	0.26	0.12	0.26
Paddy cultivation and growth	Ave	0.18	0.21	0.42	0.39	3.45	3.76	−0.05	0.02	−0.34
	Min	0.04	0.05	0.05	0.05	0.29	0.53	−0.70	−1.01	−1.93
	Max	0.63	0.69	15.21	12.40	14.32	15.85	0.42	0.44	0.50
Top dressing	Ave	0.23	0.19	0.24	0.22	2.78	3.02	0.05	0.03	−0.29
	Min	0.05	0.05	0.05	0.05	0.49	0.63	−0.34	−0.37	−3.26
	Max	1.21	0.51	1.57	1.31	9.59	9.49	0.57	1.27	0.09

Note that Ave, Min, and Max represent the average, minimum, and maximum, respectively. Moreover, 0.2–0.3 and 1.6 m represent the lower and upper levels, respectively.

The fluxes ($F_{\mathrm{HONO,\ NO,\ and\ NO_2}}$) of trace gases at the geometric mean height can be expressed as

$$F_{\mathrm{HONO,\ NO,\ and\ NO_2}} = -\kappa \cdot u_* \cdot \frac{\partial c\,(\mathrm{HONO,\ NO\ and\ NO_2})}{\partial \left[\ln(z-d) - \Psi_{\mathrm{H}}\left(\frac{z-d}{L}\right)\right]}, \quad (3)$$

where κ is the von Kármán constant ($\kappa = 0.4$), z is the height above the ground, d is the zero-plane displacement (taken as $2/3 \cdot h_c$, where h_c is the canopy height), L is the Obukhov length, and Ψ_H is the integrated stability correction function for scalars (Sutton et al., 1993).

Data from all instruments could not always be collected simultaneously for flux calculations due to various factors, such as calibration, malfunction, and disturbances from agricultural activities. Consequently, the affected data were excluded when calculating fluxes. The dataset used for the determination of HONO, NO, and NO_2 fluxes comprised 68 % of the HONO data, 81 % of the NO data, and 86 % of the NO_2 data. The total uncertainty in the flux is composed of the gradient error and the friction velocity error (Laufs et al., 2017; Meng et al., 2022). The average uncertainties for HONO, NO, and NO_2 fluxes (each calculated using the median of the 25th–75th percentile range) corresponded to 11 %, 16 %, and 20 %, respectively. Furthermore, the fluxes were discarded under very stable conditions with low wind speeds and friction velocities. It is important to note that HONO, NO, and NO_2 are subject to chemical reactions, which may lead to a vertical divergence of flux between the surface and the measurement height. The influence of chemical reactions during turbulent transport was checked utilizing the Damköhler number (*DA*), as detailed in Sect. S2. The divergence caused by chemical reactions of HONO could be neglected when interpreting the potential sources of HONO and the driving factors of HONO flux. *DA* values for the NO–O_3–NO_2 triad were generally less than 1; however, a sharp increase in flux divergence occurred when *DA* values became greater than 1 (Stella et al., 2012). Additionally, the upward NO_2 flux exhibited a significant correlation ($R = 0.82$) with NO flux, suggesting that the upward NO_2 flux could be attributed to the reaction of NO and O_3. Consequently, in light of the influence of chemical reactions on the fluxes of NO and NO_2, these fluxes (5.9 % for NO flux and 10.5 % for NO_2 flux) were excluded from subsequent analysis.

3 Results and discussion

3.1 Overview of meteorological and soil parameters

Time series of meteorological parameters recorded throughout the observation period are shown in Fig. 2. The campaign weather was dominated by sunny days, with 64 % of the days having a daily maximum global radiation level above 700 W m^{-2}. Ambient temperature ranged from 17.0

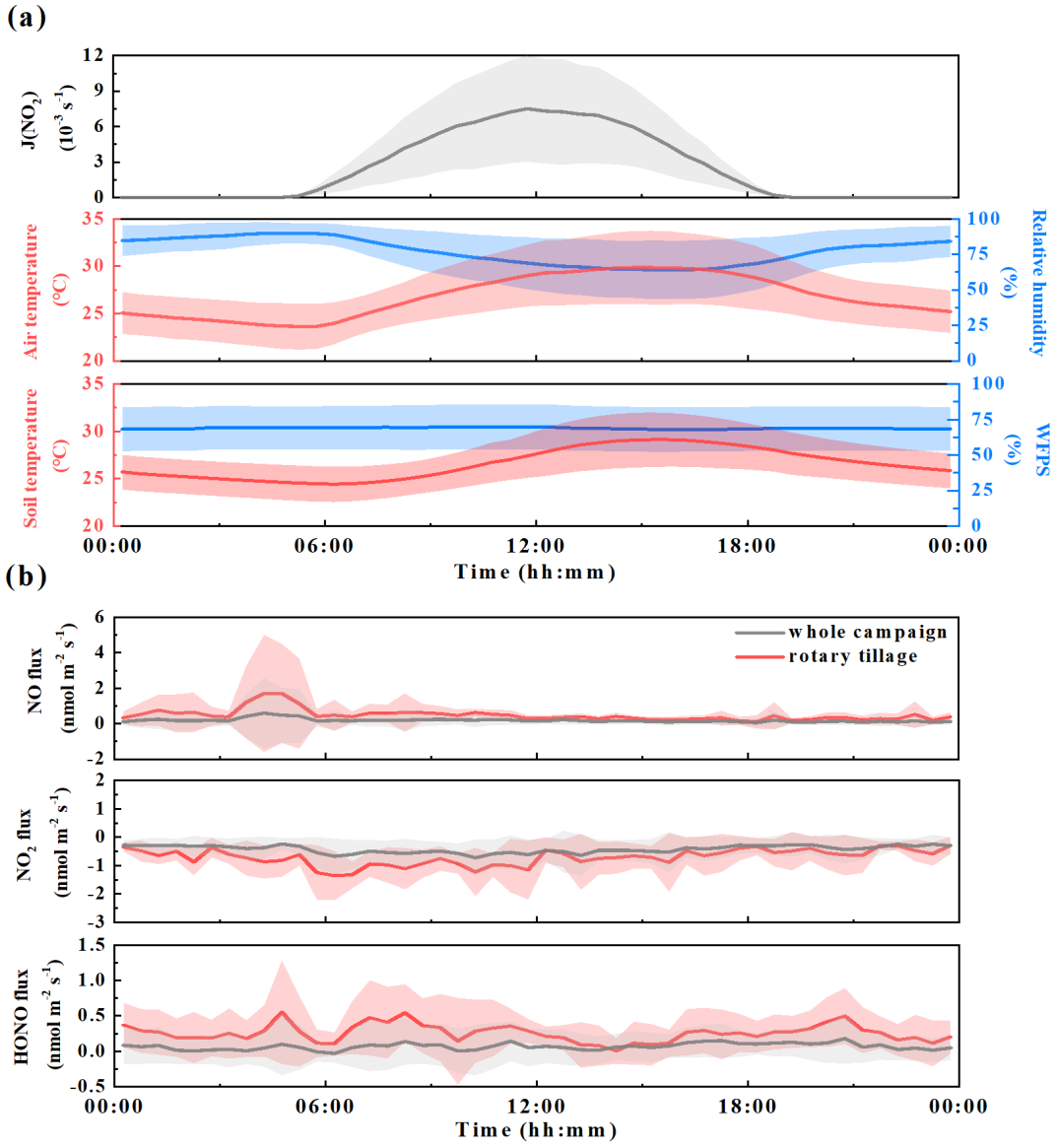

Figure 4. **(a)** Diurnal variations in NO_2 photolysis frequency ($J(NO_2)$), air temperature, relative humidity, soil temperature, and WFPS throughout the entire campaign. **(b)** Diurnal profiles of HONO, NO, and NO_2 fluxes are presented for the entire campaign and the rotary tillage period. The shaded areas denote the standard deviation.

to 36.6 °C, and soil temperature ranged from 20.0 to 34.8 °C, with average values of 26.8 ± 3.5 and 26.5 ± 2.7 °C, respectively. The relative humidity (RH) ranged from 22 % to 98 %, and the soil water-filled pore space (WFPS) ranged from 44 % to 88 %, with average values of 77 % ± 17 % and 69 % ± 15 %, respectively. The average wind speed was 3 m s^{-1}, with a maximum wind speed of 11.0 m s^{-1} occurring during the rotary tillage period. The $PM_{2.5}$ concentration varied from 1 to 100 µg m^{-3}, with its daily average value remaining below the Class II threshold of the Chinese National Ambient Air Quality Standard (75 µg m^{-3}). Intermittent rainfall occurred from 13 June to 5 July, with a total precipitation amount of 186.1 mm. Notably, after irrigation of the agricultural field on 13 June, the WFPS increased from 45 % to 80 %.

3.2 Mixing-ratio differences and fluxes of HONO, NO, and NO_2

The field campaign was conducted across various agricultural-management activities, including rotary tillage (2–13 June), flood irrigation (13–19 June), fertilization (19–21 June), paddy cultivation (26–27 June), and top dressing (10 July). Figure 3 illustrates the time series of HONO, NO, NO_2, and O_3 mixing ratios. Throughout the campaign, ambient O_3 concentrations varied from 0.54 to

Table 2. Summary of the maximum and minimum HONO fluxes in field measurements across different soil types at remote, rural, and suburban sites.

Soil type	Method	HONO flux[a] ($nmol\,m^{-2}\,s^{-1}$)		HONO flux[b] ($nmol\,m^{-2}\,s^{-1}$)		Reference
		Min	Max	Min	Max	
Grassland	AG	−0.09	0.53	–	–	Harrison and Kitto (1994)
		−0.21	0.70			
Forest	AG	0.02	0.07	–	–	Sörgel et al. (2015)
Maize	AG	–	–	0.01	0.16	Laufs et al. (2017)
Wheat	AG	−0.39	1.10	−0.003	0.20	Meng et al. (2022)
Agricultural field	REA	−0.30	0.50	−0.007	0.10	Ren et al. (2011)
Forest	REA	−0.50	1.31	0.03	0.19	Zhou et al. (2011)
Forest	REA	0.03	0.19	–	–	Zhang et al. (2012)
Grassland	REA	−0.06	0.16	0.02	0.07	Von der Heyden et al. (2022)
Maize	OTDC	0.04	0.23	–	–	Xue et al. (2019)
		0.41	2.89	–	–	
		–	108.21	–	–	
Maize	OTDC	–	2.84	-0.06	1.45	Tang et al. (2019)
Wheat	OTDC	−0.09	0.55	–	–	Tang et al. (2020)
Maize	OTDC	−0.61	22.79	0.01	10.86	Song et al. (2023)
Maize	OTDC	–	0.33	–	–	Xue et al. (2024)
		–	11.50	–	–	
		–	24.86	–	–	
Paddy	AG	−0.70	1.86	0.01	0.15	This study

AG: aerodynamic gradient. REA: relaxed eddy accumulation. OTDC: open-top dynamic chamber. [a] Values in the time series. [b] Values in the diurnal variations.

131.57 ppbv, with an average of 48.44 ± 26.29 ppbv. The peak NO mixing ratio reached 36.02 ppbv during rotary tillage, and the average mixing ratios of NO at lower (0.2–0.3 m) and upper (1.6 m) levels were 0.75 ± 2.21 and 0.46 ± 1.16 ppbv, respectively. Higher NO mixing ratios were measured at the lower level, likely due to soil NO emissions caused by microbiological activity (Bargsten et al., 2010; Ludwig et al., 2001). Moreover, the average NO_2 mixing ratios were 4.48 ± 4.96 and 4.75 ± 4.38 ppbv at the lower and upper levels, respectively. The synchronous peaks of NO and NO_2 and the decrease in O_3 (e.g., in the early hours of 7 June) indicate that NO release from soil may react rapidly with O_3 to form NO_2. Ambient HONO mixing ratios ranged from below detection limits to 3.60 ppbv at the lower level and 2.36 ppbv at the upper level, with averages of 0.46 ± 0.59 and 0.37 ± 0.37 ppbv, respectively. The average HONO / NO_x ratio of 0.079 ± 0.059 was significantly higher than the values in the range for direct emissions from vehicle exhausts, as reported in previous studies (0.003–0.018) (Kirchstetter et al., 1996; Kurtenbach et al., 2001; Liang et al., 2017; Liu et al., 2017; Nakashima and Kajii, 2017; Nakashima and Kondo, 2022), and was comparable to the value observed for summer agricultural fields in the NCP (0.0929; Song et al., 2022). Notably, successive HONO peaks were measured during rotary tillage, with HONO mixing ratios reaching 3.60 ppbv at the lower level. These values exceeded those observed during the winter at the same site (Meng et al., 2022) and were comparable to observations at suburban sites in the Pearl River Delta (Li et al., 2012; Su et al., 2008) and those at rural sites in the NCP (Xue et al., 2020). However, HONO levels declined rapidly following flood irrigation (see Fig. 3 and Table 1). After fertilization and top dressing, a noticeable rise in HONO levels was observed, which can be attributed to the increase in HONO release due to fertilizer application at high levels of water content (Tang et al., 2019; Wang et al., 2021; Wu et al., 2019; Xue et al., 2019). Nevertheless, these levels were significantly lower than the mixing ratios observed during rotary tillage.

The fluxes of HONO, NO, and NO_2 determined by the AG method are illustrated in Fig. 3. Upward fluxes were commonly observed for HONO and NO, while NO_2 was de-

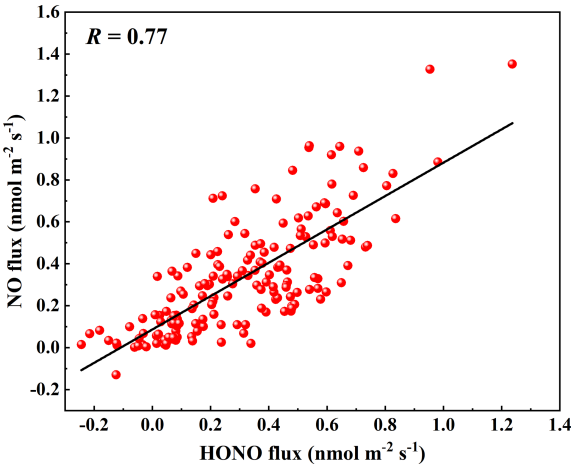

Figure 5. Correlation of HONO flux with NO flux during rotary tillage.

posited on the ground. The magnitude of observed HONO fluxes ranged from −0.70 to 1.86 nmol m^{-2} s^{-1}, with an average of 0.07 ± 0.22 nmol m^{-2} s^{-1}, which falls within the range of HONO flux measurements for rural and suburban regions reported in the literature (see Table 2). Upward HONO fluxes were mostly observed during rotary tillage, reaching up to 1.86 nmol m^{-2} s^{-1}. After irrigation, an increase in soil moisture content (∼ 80 % WFPS) led to a significant reduction in HONO flux. Previous laboratory studies have also demonstrated that lower levels of HONO flux at high water-holding capacities, low gas diffusion rates, and high solubility levels could limit the release of HONO from soil (Ermel et al., 2018; Meusel et al., 2018; Wu et al., 2014). Observations from before and after irrigation demonstrate the regulatory role of soil moisture in the HONO exchange process, which has been systematically investigated in previous studies by examining HONO emission flux as a function of soil moisture (Mamtimin et al., 2016; Wang et al., 2021). Soil moisture determines whether nitrification or denitrification processes dominate gas emissions and strongly influences the corresponding gas emission rates and concentration compensation points (Cheng, 2013). Several laboratory findings indicate that nitrification under conditions of low soil moisture is the dominant process behind HONO emissions (Oswald et al., 2013; Scharko et al., 2015), and field observations of HONO have predominantly focused on dryland ecosystems (Ren et al., 2011). Conversely, Wu et al. (2019) demonstrated that soil with a high water content (with a 75 %–140 % water-holding capacity (WHC)) can also exhibit substantial emissions of HONO, with the average ratio of the highest HONO flux during the wet peak to that during the dry peak being approximately 30 %. However, actual field observations have revealed that HONO fluxes are very low (close to zero) under conditions of high water content, which may be attributed to the influence of soil moisture on microbial metabolic activity and gas diffusion in the soil (Hu et al., 2015; Linn and Doran, 1984). Furthermore, Wang et al. (2021) reported the promoting effect of fertilization on HONO flux under conditions of high soil moisture (75 %–95 % WHC). Nevertheless, we did not observe this phenomenon in our field experiments conducted in paddy fields. This discrepancy is probably attributed to the anaerobic or microaerobic conditions created by pre-fertilization irrigation, which exerted a greater inhibitory effect on the nitrification process than the promoting effect of fertilization. Currently, the estimation of HONO flux at the regional scale relies more on laboratory research findings (Gan et al., 2024; Wu et al., 2022). This study highlights discrepancies between laboratory and field observations corresponding to high levels of soil water content, which pose significant challenges to the uncertainty in estimation results.

The agricultural field acted as a well-known source of atmospheric NO, with an average flux of 0.19 ± 0.53 nmol m^{-2} s^{-1} observed in this study. Similar to HONO fluxes, upward NO fluxes were mostly observed during rotary tillage, with a maximum flux of 9.12 nmol m^{-2} s^{-1} during the early morning (Table 1). This finding is consistent with previous studies that show that tillage increases NO emissions (Chatskikh and Olesen, 2007; Fang et al., 2006; Fang and Yujing, 2009; Liu et al., 2005; Pinto et al., 2004; Sehy et al., 2003; Yao et al., 2009; Yamulki and Jarvis, 2002). However, the NO fluxes were close to zero when the paddy field was waterlogged, probably because the nitrification process that dominates NO production in soil was greatly hindered in water-saturated soil and at anoxic microsites (Fang and Yujing, 2009). Similarly, we also did not observe significant emissions of HONO under sustained conditions of high moisture. The coinciding peaks in HONO flux and NO flux during rotary tillage suggest that HONO release from soil, similar to NO release, is associated with microbial activity in the soil (Bargsten et al., 2010; Skiba et al., 1993). Furthermore, notably elevated fluxes of HONO and NO were observed during rotary tillage compared to other phases of agricultural activities (Fig. S3). The higher emission rates of NO and HONO may account for the successive peaks in their concentrations and fluxes. Similar to NO emission, the emission of HONO from soil may be significantly stimulated by soil tillage. Additionally, an average NO_2 flux of -0.42 ± 0.44 nmol m^{-2} s^{-1} (with flux values ranging from −3.50 to 0.50 nmol m^{-2} s^{-1}) indicates that the agricultural field acted as a sink for atmospheric NO_2 (Fang and Yujing, 2009; Tang et al., 2020).

3.3 Diurnal profiles of fluxes and HONO sources during rotary tillage

Diurnal variations in NO_2 photolysis frequency ($J(NO_2)$), air temperature, relative humidity, soil temperature, WFPS, NO flux, NO_2 flux, and HONO flux are illustrated in Fig. 4. The diurnal HONO flux exhibited no discernible diurnal

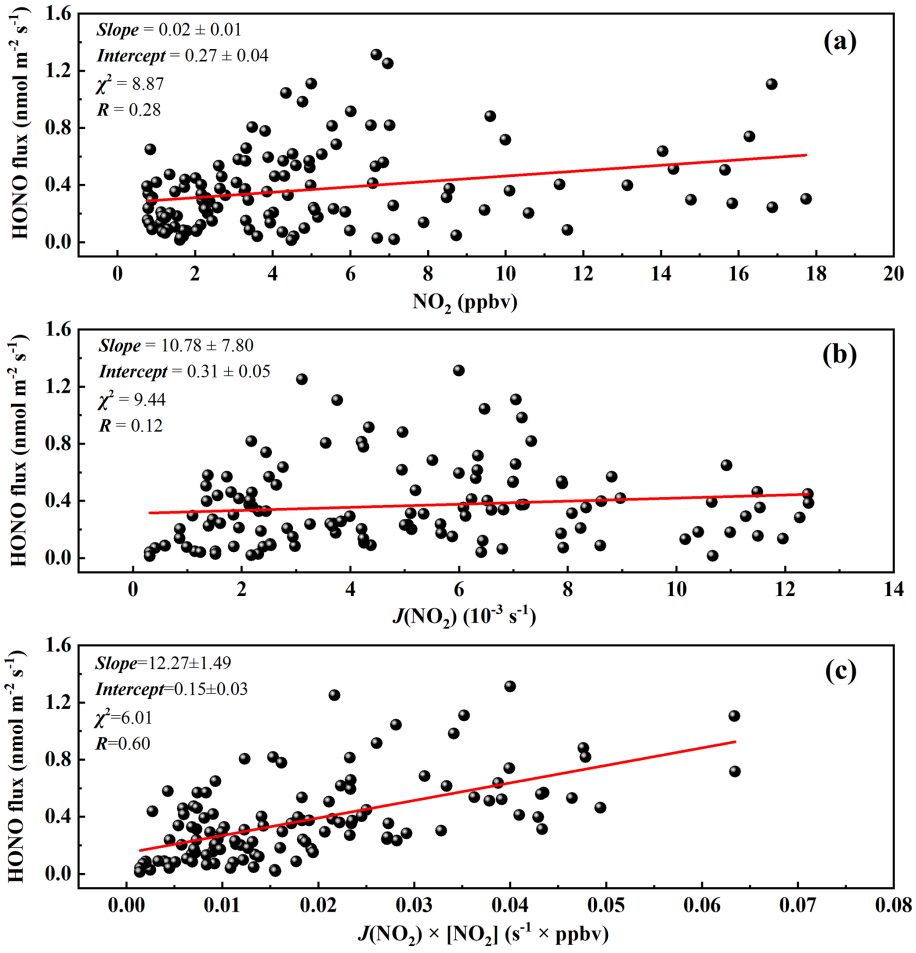

Figure 6. Correlation of daytime HONO flux with **(a)** NO_2, **(b)** $J(NO_2)$, and **(c)** the product of $J(NO_2) \times [NO_2]$ during rotary tillage.

pattern throughout the entire campaign, similar to the diurnal profile observed during BEARPEX 2009 in California (Ren et al., 2011). Significant HONO emissions were primarily observed during rotary tillage, and their daily pattern is depicted in Fig. 4. Upward HONO fluxes were observed throughout the day, with a maximum value of $0.55\,nmol\,m^{-2}\,s^{-1}$ in the early morning. Distinct HONO emissions were observed in the morning after sunrise. Moreover, the magnitudes of the daytime fluxes ($0.25 \pm 0.13\,nmol\,m^{-2}\,s^{-1}$) were comparable to the nocturnal values ($0.27 \pm 0.13\,nmol\,m^{-2}\,s^{-1}$). The diurnal profile of NO flux exhibited consistent levels of NO emissions throughout the day, except during a noticeable peak in the early morning. It is worth noting that synchronous peaks in HONO flux and NO flux were observed in the morning. Unlike for the fluxes of HONO and NO, deposition was the prevailing process for NO_2 flux. A greater downward NO_2 flux of $-0.85 \pm 0.27\,nmol\,m^{-2}\,s^{-1}$ ($-0.57 \pm 0.23\,nmol\,m^{-2}\,s^{-1}$ at night) was observed during the daytime, potentially due to an increase in the dry-deposition velocity of NO_2 during the day.

Throughout the rotary tillage period, the emissions of HONO and NO were significant, with maximum fluxes reaching $1.86\,nmol\,m^{-2}\,s^{-1}$ for HONO and $9.12\,nmol\,m^{-2}\,s^{-1}$ for NO. The concurrent peaks in HONO and NO fluxes indicate that HONO emissions may originate from soil sources as it is well established that NO is primarily generated by and released from soil microbial processes (Feig et al., 2008; Rende et al., 1989). As shown in Fig. 5, a significant correlation ($R = 0.77$) was observed between the fluxes of HONO and NO during the rotary tillage period, suggesting a shared source for both gases. This could be attributed to the generation and release of HONO and NO via soil microbial processes, aligning with the results reported by Tang et al. (2020). A Gaussian fitting was employed to analyze variations in HONO and NO fluxes with soil temperature (Fig. S4). It was found that both HONO and NO exhibited maximum emission fluxes at approximately 25 and 24 °C, respectively, which correspond to the optimal temperature (25 °C) for soil microbial nitrification and denitrification processes (Agehara and Warncke, 2005; Fang and Yujing, 2009). This finding

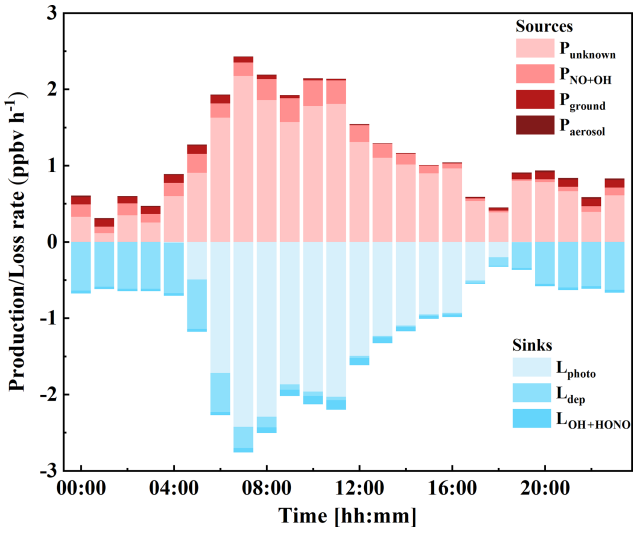

Figure 7. Diurnal variation in the HONO budget during rotary tillage.

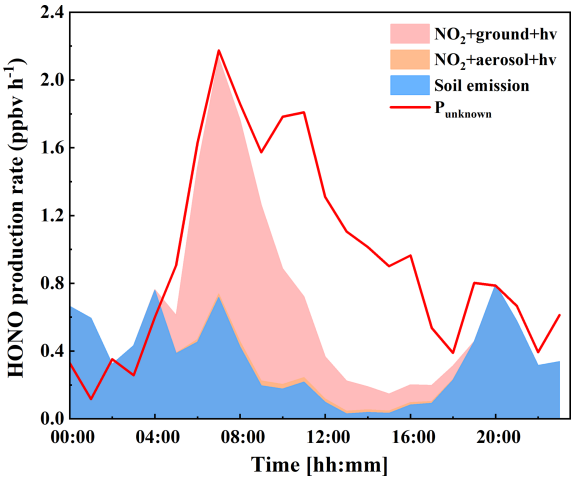

Figure 8. Diurnal variation in the light-induced conversion of NO_2 and HONO flux rates derived from soil emissions.

further supports the hypothesis that HONO is generated by and released from soil biological processes. Additionally, there was an indication of an elevation in HONO flux during periods of intense solar radiation in the morning. Although the correlations between HONO flux and NO_2, $J(NO_2)$, or NO_2 fluxes were found to be low ($R = 0.28$, 0.12, and 0.25, respectively), we observed a significant correlation ($R = 0.60$) between HONO flux and the product of $J(NO_2)$ $\times$ NO_2 (Fig. 6), as well as a moderate correlation ($R = 0.41$) between HONO flux and the product of $J(NO_2) \times NO_2$ flux (Fig. S5). This indicates that light-induced NO_2 conversion serves as an important source of HONO during the day. Furthermore, another mechanism of acid displacement can be ruled out as the major strong acid, HNO_3, is primarily generated during the daytime and subsequently deposited on the ground. Consequently, the peak of the HONO source is expected to occur in the afternoon (Vandenboer et al., 2015). Finally, the results indicate that both mechanisms – release from soil biological processes and that from light-induced NO_2 conversion – are likely active, together affecting the diurnal HONO flux pattern.

3.4 HONO budget during rotary tillage

In Sect. 3.3, we presented the potential sources of HONO flux during rotary tillage by conducting a correlation analysis. Here, we will further calculate the specific contributions of HONO sources through a budget analysis. The HONO budget can be derived from known HONO sources and sinks, and the potential unknown HONO source during rotary tillage was estimated. The lower-level data that better describe ground source processes were used for the budget analysis. In this study, the investigated HONO sources included the homogeneous reaction (P_{OH+NO}) and the heterogeneous reactions of NO_2 on the aerosol surface and that on the ground surface ($P_{aerosol}$ and P_{ground}, respectively). The HONO sinks included the reaction of HONO with OH ($L_{OH+HONO}$), the photolysis of HONO (L_{photo}), and the dry-deposition loss of HONO (L_{dep}). The calculations of HONO sources and sinks, as well as the estimates of the mixing-layer height (MLH), are described in detail in Sect. S3.

$$\frac{\mathrm{dHONO}}{\mathrm{d}t} = \left(P_{OH+NO} + P_{unknown} + P_{aerosol} + P_{ground}\right) - \left(L_{OH+HONO} + L_{photo} + L_{dep}\right) \quad (4)$$

Simplifying Eq. (4), $\mathrm{dHONO}/\mathrm{d}t$ is approximated by $\Delta\mathrm{HONO}/\Delta t$. Then, Eq. (4) becomes Eq. (5) as follows:

$$P_{unknown} = \frac{\Delta\mathrm{HONO}}{\Delta t} + L_{OH+HONO} + L_{photo} + L_{dep} - P_{OH+NO} - P_{aerosol} - P_{ground}\,. \quad (5)$$

The average production and loss rates for the diurnal HONO budget are shown in Fig. 7. The homogeneous reaction of NO and OH accounted for 12.8 % of HONO production, with an average P_{OH+NO} value of 0.15 ± 0.10 ppbv h^{-1}. The heterogeneous conversion of NO_2 on the ground surface accounted for 12.4 % (0.1 ± 0.07 ppbv h^{-1}) of HONO production at night. $P_{aerosol}$ (0.01 ± 0.006 ppbv h^{-1}) was negligible compared to other HONO sources due to its relatively small aerosol surface area (Fig. S6). Photodecomposition (L_{photo}) was the primary sink of HONO during the daytime, with a peak of 2.03 ppbv h^{-1} at 11:00 and an average of 1.44 ± 0.69 ppbv h^{-1}, while $L_{OH+HONO}$ was very small and accounted for less than 5 % of L_{photo}. The dry deposition of HONO (L_{dep}) was influenced by the mixing-layer height (MLH) and dominated the loss of HONO at night, with a rate exceeding 0.6 ppbv h^{-1}. $P_{unknown}$ exhibited an obvious diurnal variation, with higher values during

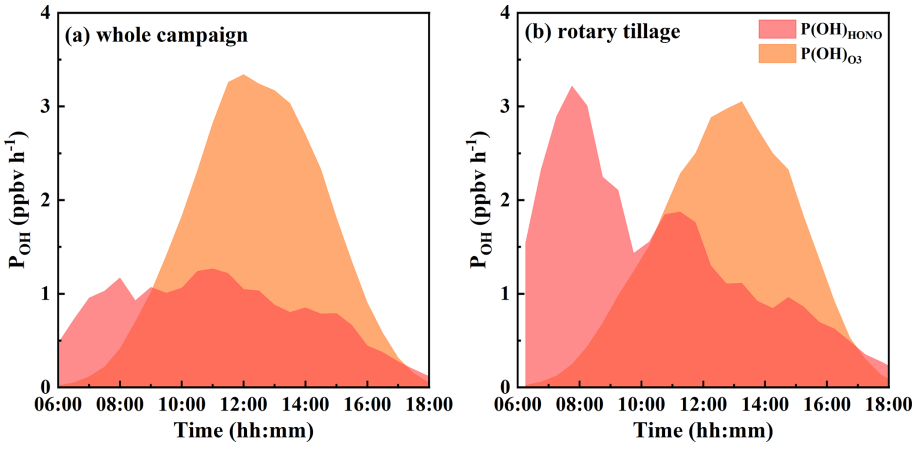

Figure 9. Diurnal variation in net OH production rates from the photolysis of HONO ($P(\mathrm{OH})_{\mathrm{HONO}}$) and O_3 ($P(\mathrm{OH})_{\mathrm{O_3}}$) during **(a)** the entire campaign and **(b)** rotary tillage.

the daytime (1.31 ± 0.54 ppbv h^{-1}) and lower values at night (0.53 ± 0.25 ppbv h^{-1}). The peak of P_{unknown} occurred from 07:00–12:00, with a maximum value of 2.18 ppb h^{-1}. The peak value of P_{unknown} is comparable to the value measured in Taizhou (2.5 ppbv h^{-1}) (Ye et al., 2023) and larger than the values measured in Wangdu (0.62 ppbv h^{-1}) (Song et al., 2022) and Nanjing (1.04 ppbv h^{-1}) (Liu et al., 2019a). Similar to the observed asymmetry around noon reported in previous studies, this could be attributed to the combined effect of solar radiation and variations in precursor NO_2 (Song et al., 2022; Xue et al., 2022). Due to the significantly larger unknown source strength of HONO during the daytime, we focused on analyzing the unknown source of HONO during the day. Based on the above analysis, we evaluated the contribution of the photo-enhanced heterogeneous pathways.

The coefficients widely adopted in previous studies generally range from 10^{-6} to 10^{-4} (Chen et al., 2023; Liu et al., 2019b; Song et al., 2022; Wong et al., 2013). Here, we used 1×10^{-5} for the photo-enhanced uptake coefficients (γ_{a+hv} and γ_{g+hv}) to calculate $P_{\mathrm{aerosol}+hv}$ and $P_{\mathrm{ground}+hv}$ (Qin et al., 2023; Xue et al., 2020). As shown in Fig. 8, the average $P_{\mathrm{aerosol}+hv}$ and $P_{\mathrm{ground}+hv}$ values were 0.02 ± 0.009 and 0.53 ± 0.50 ppbv h^{-1}, respectively, during the day, accounting for 1.4 % and 40.2 % of P_{unknown}, respectively. Moreover, $P_{\mathrm{aerosol}+hv}$ was a negligible source of daytime HONO formation. The photo-enhanced NO_2 heterogeneous reaction on the surface matched the calculated P_{unknown} value and effectively explained the HONO budget for the morning. Furthermore, a higher photo-enhanced uptake coefficient of 3.5×10^{-5} was adopted as the upper limit for calculating the production of the photosensitive conversion of NO_2 (Chen et al., 2023). The calculation results demonstrated that the daytime value of P_{unknown} could be explained when the upper limit of the photo-enhanced uptake coefficient was used (Fig. S8).

However, there could be other light-driven reaction pathways for producing HONO in the afternoon, as indicated by the diurnal variation in P_{unknown}. Previous studies have demonstrated that the photolysis of pNO_3 / HNO_3 can contribute to HONO production (Chen et al., 2023; Laufs et al., 2017). Recently, Chen et al. (2023) found that the photolysis of HNO_3 at the surface interface could effectively explain the observed P_{unknown} value for the afternoon. However, the lack of information about HNO_3 concentration prevents us from directly estimating the contribution of HNO_3 photolysis in the present study. Future studies should include measurements of pNO_3 / HNO_3 to better characterize the contribution of this potentially important HONO formation pathway.

Based on the measured fluxes, we also estimated the HONO emission rate from soil (P_{soil}). The nighttime HONO fluxes ranged from 0.15 to 0.43 nmol m^{-2} s^{-1}, with corresponding HONO flux rates of 0.32 to 0.79 ppbv h^{-1}; these values were sufficient for explaining P_{unknown} (ranging from 0.012 to 0.90 ppbv h^{-1}). Therefore, light-induced HONO sources (i.e., the photosensitive conversion of NO_2 and photolysis of pNO_3 / HNO_3) and soil emissions may together serve as significant HONO sources in agricultural fields, thereby influencing the overall atmospheric HONO budget.

3.5 Implications for atmospheric oxidizing capacity

The significant increase in atmospheric HONO from agricultural fields can enhance the formation of OH radicals via the photolysis of HONO (see the detailed OH production rate calculation in Sect. S4). Figure 9a exhibits the OH production rates from the photolysis of HONO ($P(\mathrm{OH})_{\mathrm{HONO}}$) and O_3 ($P(\mathrm{OH})_{\mathrm{O_3}}$). $P(\mathrm{OH})_{\mathrm{HONO}}$ and $P(\mathrm{OH})_{\mathrm{O_3}}$ were found to be 0.82 and 1.49 ppbv h^{-1}, respectively, meaning they were significantly higher than the corresponding winter levels at the same site (Fig. S9). The higher O_3 concentration in summer plays a primary role in the generation of OH radicals through daytime O_3 photolysis, accounting for 70 % of the total OH production rate. However, the contribution of $P(\mathrm{OH})_{\mathrm{HONO}}$,

approximately 30 %, is still significant and cannot be ignored.

During the rotary tillage period, continuous peaks in HONO concentration and flux were observed, with maximum values of 3.06 ppbv and 1.86 nmol m^{-2} s^{-1}, respectively. $P(OH)_{HONO}$ was calculated to be 1.42 ppbv h^{-1}, and $P(OH)_{O_3}$ was determined to be 1.35 ppbv h^{-1}, accounting for 51 % and 49 % of the total OH production rate, respectively (Fig. 9b). $P(OH)_{HONO}$ dominated in the early morning, with a value of 2.48 ppbv h^{-1}, while $P(OH)_{O_3}$ became the main source at midday, with a value of 2.74 ppbv h^{-1}. The comparable peak magnitudes of $P(OH)_{HONO}$ and $P(OH)_{O_3}$ indicate that HONO photolysis is an important source of daytime OH radicals. Furthermore, the peaks in both $P(OH)_{HONO}$ and HONO flux co-occur in the early morning, revealing the significant contribution of agricultural HONO emissions to the regional atmospheric oxidation capacity of the Huaihe River Basin.

4 Conclusions

Extensive agricultural fields and increased agricultural activity have contributed to certain areas in China becoming hotspots for atmospheric nitrogen oxides, underscoring the increasing importance of regional and global nitrogen budgets. However, available HONO emission flux data from agricultural soils are relatively limited. In this study, we utilized the AG method to measure HONO and NO_x fluxes from agricultural fields in the Huaihe River Basin. For HONO and NO, upward fluxes of 0.07 ± 0.22 and 0.19 ± 0.53 nmol m^{-2} s^{-1}, respectively, were observed, while NO_2 exhibited a deposition flux to the ground of -0.42 ± 0.44 nmol m^{-2} s^{-1}. The successive peaks in HONO and NO fluxes were measured during rotary tillage, suggesting a potentially enhanced release of HONO and NO due to soil tillage activities. However, an increased WFPS inhibited microbial nitrification processes after irrigation, leading to a significant decrease in HONO and NO fluxes. Under this inhibitory effect, no significant peaks in HONO flux were observed after fertilization, in contrast to those observed during rotary tillage. Considering the limited field observations of HONO flux under high levels of soil water content, future studies should pay more attention to paddy fields to validate the mechanisms observed in the laboratory.

Significant fluxes were observed during rotary tillage, prompting an investigation into the sources and budget of HONO during this period. Biological processes and light-driven NO_2 reactions on the ground surface may both be sources of HONO and influence the local HONO budget. Higher levels of $P(OH)_{HONO}$ were observed in the early morning, consistent with the peak emission flux of soil HONO. This reveals the significant contribution of agricultural HONO emissions to the regional atmospheric oxidation capacity of the Huaihe River Basin. Overall, this study provides valuable insights into the dynamics of soil HONO emissions in agricultural fields, elucidating their environmental implications and the role of agricultural activities in the atmospheric chemistry of HONO.

Data availability. The data described in this paper are available at https://doi.org/10.5281/zenodo.14016614 (Meng et al., 2024) or upon request from the corresponding author (mqin@aiofm.ac.cn).

Supplement. The supplement related to this article is available online at: https://doi.org/10.5194/acp-24-14191-2024-supplement.

Author contributions. MQ and PX designed the experiments. FM, KT, DS, ZL, and JD performed the measurements. FM and BH analyzed the data and wrote the paper. MQ revised and commented on the paper. YF, YH, and TN provided the ancillary data and experimental sites.

Competing interests. The contact author has declared that none of the authors has any competing interests.

Disclaimer. Publisher's note: Copernicus Publications remains neutral with regard to jurisdictional claims made in the text, published maps, institutional affiliations, or any other geographical representation in this paper. While Copernicus Publications makes every effort to include appropriate place names, the final responsibility lies with the authors.

Acknowledgements. The authors thank the Shouxian National Climatology Observatory for providing the field experimental site and auxiliary data.

Financial support. This research has been supported by the National Key Research and Development Program of China (grant no. 2022YFC3701103), the National Natural Science Foundation of China (grant nos. U21A2028 and 41875154), and the Major Science and Technology Projects in Anhui Province (grant no. 202203a07020003).

Review statement. This paper was edited by Tao Wang and reviewed by two anonymous referees.

References

Agehara, S. and Warncke, D. D.: Soil Moisture and Temperature Effects on Nitrogen Release from Organic Nitrogen Sources, Soil Sci. Soc. Am. J., 69, 1844–1855, https://doi.org/10.2136/sssaj2004.0361, 2005.

Bargsten, A., Falge, E., Pritsch, K., Huwe, B., and Meixner, F. X.: Laboratory measurements of nitric oxide release from forest soil with a thick organic layer under different understory types, Biogeosciences, 7, 1425–1441, https://doi.org/10.5194/bg-7-1425-2010, 2010.

Bejan, I., Abd El Aal, Y., Barnes, I., Benter, T., Bohn, B., Wiesen, P., and Kleffmann, J.: The photolysis of ortho-nitrophenols: a new gas phase source of HONO, Phys. Chem. Chem. Phys., 8, 2028–2035, https://doi.org/10.1039/b516590c, 2006.

Bhattarai, H. R., Wanek, W., Siljanen, H. M. P., Ronkainen, J. G., Liimatainen, M., Hu, Y., Nykänen, H., Biasi, C., and Maljanen, M.: Denitrification is the major nitrous acid production pathway in boreal agricultural soils, Commun. Earth Environ., 2, 54, https://doi.org/10.1038/s43247-021-00125-7, 2021.

Cao, Q., Hao, Z., Yuan, F., Berndtsson, R., Xu, S., Gao, H., and Hao, J.: On the Predictability of Daily Rainfall during Rainy Season over the Huaihe River Basin, Water, 11, 916, https://doi.org/10.3390/w11050916, 2019.

Chatskikh, D. and Olesen, J. E.: Soil tillage enhanced CO_2 and N_2O emissions from loamy sand soil under spring barley, Soil Till. Res., 97, 5–18, https://doi.org/10.1016/j.still.2007.08.004, 2007.

Chen, D., Zhou, L., Liu, S., Lian, C., Wang, W., Liu, H., Li, C., Liu, Y., Luo, L., Xiao, K., Chen, Y., Qiu, Y., Tan, Q., Ge, M., and Yang, F.: Primary sources of HONO vary during the daytime: Insights based on a field campaign, Sci. Total Environ., 903, 166605, https://doi.org/10.1016/j.scitotenv.2023.166605, 2023.

Cheng, P.: Measurement of the atmospheric nitrous acid (HONO) and the study of its soil emissions, PhD Thesis, Peking University, China, 125 pp., 2013.

Duan, J., Qin, M., Ouyang, B., Fang, W., Li, X., Lu, K., Tang, K., Liang, S., Meng, F., Hu, Z., Xie, P., Liu, W., and Häsler, R.: Development of an incoherent broadband cavity-enhanced absorption spectrometer for in situ measurements of HONO and NO_2, Atmos. Meas. Tech., 11, 4531–4543, https://doi.org/10.5194/amt-11-4531-2018, 2018.

Elshorbany, Y. F., Kleffmann, J., Kurtenbach, R., Rubio, M., Lissi, E., Villena, G., Gramsch, E., Rickard, A. R., Pilling, M. J., and Wiesen, P.: Summertime photochemical ozone formation in Santiago, Chile, Atmos. Environ., 43, 6398–6407, https://doi.org/10.1016/j.atmosenv.2009.08.047, 2009.

Ermel, M., Behrendt, T., Oswald, R., Derstroff, B., Wu, D., Hohlmann, S., Stönner, C., Pommerening-Röser, A., Könneke, M., Williams, J., Meixner, F. X., Andreae, M. O., Trebs, I., and Sörgel, M.: Hydroxylamine released by nitrifying microorganisms is a precursor for HONO emission from drying soils, Sci. Rep., 8, 1877, https://doi.org/10.1038/s41598-018-20170-1, 2018.

Fang, S. and Yujing, M.: NO_x fluxes from several typical agricultural fields during summer-autumn in the Yangtze Delta, China, Atmos. Environ., 43, 2665–2671, https://doi.org/10.1016/j.atmosenv.2009.02.027, 2009.

Fang, S., Zhang, Y., and Mu, Y.: Surface-exchange of NO_x and NH_3 above a winter wheat field in the Yangtze Delta, China, J. Environ. Sci., 18, 689–700, 2006.

FAO: World Food and Agriculture – Statistical Yearbook 2022, Rome, https://doi.org/10.4060/cc2211en, 2022.

Feig, G. T., Mamtimin, B., and Meixner, F. X.: Soil biogenic emissions of nitric oxide from a semi-arid savanna in South Africa, Biogeosciences, 5, 1723–1738, https://doi.org/10.5194/bg-5-1723-2008, 2008.

Gan, C., Li, B., Dong, J., Li, Y., Zhao, Y., Wang, T., Yang, Y., and Liao, H.: Atmospheric HONO emissions in China: Unraveling the spatiotemporal patterns and their key influencing factors, Environ. Pollut., 343, 123228, https://doi.org/10.1016/j.envpol.2023.123228, 2024.

Ge, S., Wang, G., Zhang, S., Li, D., Xie, Y., Wu, C., Yuan, Q., Chen, J., and Zhang, H.: Abundant NH_3 in China Enhances Atmospheric HONO Production by Promoting the Heterogeneous Reaction of SO_2 with NO_2, Environ. Sci. Technol., 53, 14339–14347, https://doi.org/10.1021/acs.est.9b04196, 2019.

George, C., Strekowski, R. S., Kleffmann, J., Stemmler, K., and Ammann, M.: Photoenhanced uptake of gaseous NO_2 on solid organic compounds: A photochemical source of HONO?, Faraday Discuss., 130, 195–210, https://doi.org/10.1039/b417888m, 2005.

Guo, S. and Li, H.: Photolysis of nitrophenols in gas phase and aqueous environment: a potential daytime source for atmospheric nitrous acid (HONO), Environ. Sci.-Atmos., 3, 143–155, https://doi.org/10.1039/d2ea00053a, 2022.

Han, C., Yang, W., Wu, Q., Yang, H., and Xue, X.: Heterogeneous Photochemical Conversion of NO_2 to HONO on the Humic Acid Surface under Simulated Sunlight, Environ. Sci. Technol., 50, 5017–5023, https://doi.org/10.1021/acs.est.5b05101, 2016.

Harrison, R. M. and Kitto, A. M. N.: Evidence for a surface source of atmospheric nitrous acid, Atmos. Environ., 28, 1089–1094, https://doi.org/10.1016/1352-2310(94)90286-0, 1994.

Hu, H. W., Macdonald, C. A., Trivedi, P., Holmes, B., Bodrossy, L., He, J. Z., and Singh, B. K.: Water addition regulates the metabolic activity of ammonia oxidizers responding to environmental perturbations in dry subhumid ecosystems, Environ. Microbiol., 17, 444–461, https://doi.org/10.1111/1462-2920.12481, 2015.

Kim, S., Vandenboer, T. C., Young, C. J., Riedel, T. P., Thornton, J. A., Swarthout, B., Sive, B., Lerner, B., Gilman, J., Warneke, C., Roberts, J. M., Guenther, A., Wagner, N. L., Dubé, W. P., Williams, E., and Brown, S. S.: The primary and recycling sources of OH during the NACHTT-2011 campaign: HONO as an important OH primary source in the wintertime, J. Geophys. Res., 119, 6886–6896, https://doi.org/10.1002/2013JD019784, 2014.

Kirchstetter, T. W., Harley, R. A., and Littlejohn, D.: Measurement of nitrous acid in motor vehicle exhaust, Environ. Sci. Technol., 30, 2843–2849, https://doi.org/10.1021/es960135y, 1996.

Kleffmann, J., Gavriloaiei, T., Hofzumahaus, A., Holland, F., Koppmann, R., Rupp, L., Schlosser, E., Siese, M., and Wahner, A.: Daytime formation of nitrous acid: A major source of OH radicals in a forest, Geophys. Res. Lett., 32, 1–4, https://doi.org/10.1029/2005GL022524, 2005.

Kratz, A. M., Maier, S., Weber, J., Kim, M., Mele, G., Gargiulo, L., Leifke, A. L., Prass, M., Abed, R. M. M., Cheng, Y., Su, H., Pöschl, U., and Weber, B.: Reactive Nitrogen Hotspots Related to Microscale Heterogeneity in Biological Soil Crusts, Environ. Sci. Technol., 56, 11865–11877, https://doi.org/10.1021/acs.est.2c02207, 2022.

Kurtenbach, R., Becker, K. H., Gomes, J. A. G., Kleffmann, J., Lörzer, J. C., Spittler, M., Wiesen, P., Ackermann, R., Geyer, A., and Platt, U.: Investigations of emissions and heterogeneous

formation of HONO in a road traffic tunnel, Atmos. Environ., 35, 3385–3394, https://doi.org/10.1016/S1352-2310(01)00138-8, 2001.

Laufs, S., Cazaunau, M., Stella, P., Kurtenbach, R., Cellier, P., Mellouki, A., Loubet, B., and Kleffmann, J.: Diurnal fluxes of HONO above a crop rotation, Atmos. Chem. Phys., 17, 6907–6923, https://doi.org/10.5194/acp-17-6907-2017, 2017.

Lee, J. D., Whalley, L. K., Heard, D. E., Stone, D., Dunmore, R. E., Hamilton, J. F., Young, D. E., Allan, J. D., Laufs, S., and Kleffmann, J.: Detailed budget analysis of HONO in central London reveals a missing daytime source, Atmos. Chem. Phys., 16, 2747–2764, https://doi.org/10.5194/acp-16-2747-2016, 2016.

Li, L., Duan, Z., Li, H., Zhu, C., Henkelman, G., Francisco, J. S., and Zeng, X. C.: Formation of HONO from the NH_3-promoted hydrolysis of NO_2 dimers in the atmosphere, P. Natl. Acad. Sci. USA, 115, 7236–7241, https://doi.org/10.1073/pnas.1807719115, 2018.

Li, X., Brauers, T., Häseler, R., Bohn, B., Fuchs, H., Hofzumahaus, A., Holland, F., Lou, S., Lu, K. D., Rohrer, F., Hu, M., Zeng, L. M., Zhang, Y. H., Garland, R. M., Su, H., Nowak, A., Wiedensohler, A., Takegawa, N., Shao, M., and Wahner, A.: Exploring the atmospheric chemistry of nitrous acid (HONO) at a rural site in Southern China, Atmos. Chem. Phys., 12, 1497–1513, https://doi.org/10.5194/acp-12-1497-2012, 2012.

Liang, Y., Zha, Q., Wang, W., Cui, L., Lui, K. H., Ho, K. F., Wang, Z., Lee, S. C., and Wang, T.: Revisiting nitrous acid (HONO) emission from on-road vehicles: A tunnel study with a mixed fleet, J. Air Waste Manage., 67, 797–805, https://doi.org/10.1080/10962247.2017.1293573, 2017.

Linn, D. M. and Doran, J. W.: Effect of Water-Filled Pore Space on Carbon Dioxide and Nitrous Oxide Production in Tilled and Nontilled Soils, Soil Sci. Soc. Am. J., 48, 1267–1272, https://doi.org/10.2136/sssaj1984.03615995004800060013x, 1984.

Liu, J., Li, S., Mekic, M., Jiang, H., Zhou, W., Loisel, G., Song, W., Wang, X., and Gligorovski, S.: Photoenhanced Uptake of NO_2 and HONO Formation on Real Urban Grime, Environ. Sci. Tech. Let., 6, 413–417, https://doi.org/10.1021/acs.estlett.9b00308, 2019.

Liu, X. J., Mosier, A. R., Halvorson, A. D., and Zhang, F. S.: Tillage and nitrogen application effects on nitrous and nitric oxide emissions from irrigated corn fields, Plant Soil, 276, 235–249, https://doi.org/10.1007/s11104-005-4894-4, 2005.

Liu, Y., Lu, K., Ma, Y., Yang, X., Zhang, W., Wu, Y., Peng, J., Shuai, S., Hu, M., and Zhang, Y.: Direct emission of nitrous acid (HONO) from gasoline cars in China determined by vehicle chassis dynamometer experiments, Atmos. Environ., 169, 89–96, https://doi.org/10.1016/j.atmosenv.2017.07.019, 2017.

Liu, Y., Nie, W., Xu, Z., Wang, T., Wang, R., Li, Y., Wang, L., Chi, X., and Ding, A.: Semi-quantitative understanding of source contribution to nitrous acid (HONO) based on 1 year of continuous observation at the SORPES station in eastern China, Atmos. Chem. Phys., 19, 13289–13308, https://doi.org/10.5194/acp-19-13289-2019, 2019a.

Liu, Y., Lu, K., Li, X., Dong, H., Tan, Z., Wang, H., Zou, Q., Wu, Y., Zeng, L., Hu, M., Min, K. E., Kecorius, S., Wiedensohler, A., and Zhang, Y.: A Comprehensive Model Test of the HONO Sources Constrained to Field Measurements at Rural North China Plain, Environ. Sci. Technol., 53, 3517–3525, https://doi.org/10.1021/acs.est.8b06367, 2019b.

Ludwig, J., Meixner, F. X., Vogel, B., and Förstner, J.: Soil-air exchange of nitric oxide: An overview of processes, environmental factors, and modeling studies, Biogeochemistry, 52, 225–257, https://doi.org/10.1023/A:1006424330555, 2001.

Mamtimin, B., Meixner, F. X., Behrendt, T., Badawy, M., and Wagner, T.: The contribution of soil biogenic NO and HONO emissions from a managed hyperarid ecosystem to the regional NO_x emissions during growing season, Atmos. Chem. Phys., 16, 10175–10194, https://doi.org/10.5194/acp-16-10175-2016, 2016.

Marion, A., Morin, J., Gandolfo, A., Ormeño, E., D'Anna, B., and Wortham, H.: Nitrous acid formation on Zea mays leaves by heterogeneous reaction of nitrogen dioxide in the laboratory, Environ. Res., 193, 110543, https://doi.org/10.1016/j.envres.2020.110543, 2021.

Meng, F., Qin, M., Fang, W., Duan, J., Tang, K., Zhang, H., Shao, D., Liao, Z., Feng, Y., Huang, Y., Ni, T., Xie, P., Liu, J., and Liu, W.: Measurement of HONO flux using the aerodynamic gradient method over an agricultural field in the Huaihe River Basin, China, J. Environ. Sci., 114, 297–307, https://doi.org/10.1016/j.jes.2021.09.005, 2022.

Meng, F., Han, B., Qin, M., Fang, W., Tang, K., Shao, D., Liao, Z., Duan, J., Feng, Y., Huang, Y., Ni, T., and Xie, P.: Measurement report: Surface exchange fluxes of HONO during the growth process of paddy fields in the Huaihe River Basin, China, Zenodo [data set], https://doi.org/10.5281/zenodo.14016614, 2024.

Meusel, H., Tamm, A., Kuhn, U., Wu, D., Leifke, A. L., Fiedler, S., Ruckteschler, N., Yordanova, P., Lang-Yona, N., Pöhlker, M., Lelieveld, J., Hoffmann, T., Pöschl, U., Su, H., Weber, B., and Cheng, Y.: Emission of nitrous acid from soil and biological soil crusts represents an important source of HONO in the remote atmosphere in Cyprus, Atmos. Chem. Phys., 18, 799–813, https://doi.org/10.5194/acp-18-799-2018, 2018.

Monge, M. E., D'Anna, B., Mazri, L., Giroir-Fendler, A., Ammann, M., Donaldson, D. J., and George, C.: Light changes the atmospheric reactivity of soot, P. Natl. Acad. Sci. USA, 107, 6605–6609, https://doi.org/10.1073/pnas.0908341107, 2010.

Monks, P. S., Granier, C., Fuzzi, S., Stohl, A., Williams, M. L., Akimoto, H., Amann, M., Baklanov, A., Baltensperger, U., Bey, I., Blake, N., Blake, R. S., Carslaw, K., Cooper, O. R., Dentener, F., Fowler, D., Fragkou, E., Frost, G. J., Generoso, S., Ginoux, P., Grewe, V., Guenther, A., Hansson, H. C., Henne, S., Hjorth, J., Hofzumahaus, A., Huntrieser, H., Isaksen, I. S. A., Jenkin, M. E., Kaiser, J., Kanakidou, M., Klimont, Z., Kulmala, M., Laj, P., Lawrence, M. G., Lee, J. D., Liousse, C., Maione, M., McFiggans, G., Metzger, A., Mieville, A., Moussiopoulos, N., Orlando, J. J., O'Dowd, C. D., Palmer, P. I., Parrish, D. D., Petzold, A., Platt, U., Pöschl, U., Prévôt, A. S. H., Reeves, C. E., Reimann, S., Rudich, Y., Sellegri, K., Steinbrecher, R., Simpson, D., ten Brink, H., Theloke, J., van der Werf, G. R., Vautard, R., Vestreng, V., Vlachokostas, C., and von Glasow, R.: Atmospheric composition change – global and regional air quality, Atmos. Environ., 43, 5268–5350, https://doi.org/10.1016/j.atmosenv.2009.08.021, 2009.

Mueller, N. D., Lassaletta, L., Runck, B. C., Billen, G., Garnier, J., and Gerber, J. S.: Declining spatial efficiency of global crop-

land nitrogen allocation, Global Biogeochem. Cy., 31, 245–257, https://doi.org/10.1002/2016gb005515, 2017.

Nakashima, Y. and Kajii, Y.: Determination of nitrous acid emission factors from a gasoline vehicle using a chassis dynamometer combined with incoherent broadband cavity-enhanced absorption spectroscopy, Sci. Total Environ., 575, 287–293, https://doi.org/10.1016/j.scitotenv.2016.10.050, 2017.

Nakashima, Y. and Kondo, Y.: Nitrous acid (HONO) emission factors for diesel vehicles determined using a chassis dynamometer, Sci. Total Environ., 806, 150927, https://doi.org/10.1016/j.scitotenv.2021.150927, 2022.

Nan, J., Wang, S., Guo, Y., Xiang, Y., and Zhou, B.: Study on the daytime OH radical and implication for its relationship with fine particles over megacity of Shanghai, China, Atmos. Environ., 154, 167–178, https://doi.org/10.1016/j.atmosenv.2017.01.046, 2017.

Ndour, M., D'Anna, B., George, C., Ka, O., Balkanski, Y., Kleffmann, J., Stemmler, K., and Ammann, M.: Photoenhanced uptake of NO_2 on mineral dust: Laboratory experiments and model simulations, Geophys. Res. Lett., 35, L05812, https://doi.org/10.1029/2007gl032006, 2008.

Nie, W., Ding, A. J., Xie, Y. N., Xu, Z., Mao, H., Kerminen, V.-M., Zheng, L. F., Qi, X. M., Huang, X., Yang, X.-Q., Sun, J. N., Herrmann, E., Petäjä, T., Kulmala, M., and Fu, C. B.: Influence of biomass burning plumes on HONO chemistry in eastern China, Atmos. Chem. Phys., 15, 1147–1159, https://doi.org/10.5194/acp-15-1147-2015, 2015.

Oswald, R., Behrendt, T., Ermel, M., Wu, D., Su, H., Cheng, Y., Breuninger, C., Moravek, A., Mougin, E., Delon, C., Loubet, B., Pommerening-Roser, A., Sorgel, M., Poschl, U., Hoffmann, T., Andreae, M. O., Meixner, F. X., and Trebs, I.: HONO emissions from soil bacteria as a major source of atmospheric reactive nitrogen, Science, 341, 1233–1235, https://doi.org/10.1126/science.1242266, 2013.

Pilegaard, K.: Processes regulating nitric oxide emissions from soils, Philos. T. Roy. Soc. B, 368, 20130126, https://doi.org/10.1098/rstb.2013.0126, 2013.

Pinto, M., Merino, P., del Prado, A., Estavillo, J. M., Yamulki, S., Gebauer, G., Piertzak, S., Lauf, J., and Oenema, O.: Increased emissions of nitric oxide and nitrous oxide following tillage of a perennial pasture, Nutr. Cycl. Agroecosys., 70, 13–22, https://doi.org/10.1023/B:FRES.0000049357.79307.23, 2004.

Qin, Z., Geng, C., Xu, B., Liu, Y., Zhang, N., Zheng, Z., Wang, X., and Yang, W.: Springtime HONO budget and its impact on the O_3 production in Zibo, Shandong, China, Atmos. Pollut. Res., 15, 101935, https://doi.org/10.1016/j.apr.2023.101935, 2023.

Ren, X., Sanders, J. E., Rajendran, A., Weber, R. J., Goldstein, A. H., Pusede, S. E., Browne, E. C., Min, K.-E., and Cohen, R. C.: A relaxed eddy accumulation system for measuring vertical fluxes of nitrous acid, Atmos. Meas. Tech., 4, 2093–2103, https://doi.org/10.5194/amt-4-2093-2011, 2011.

Rende, A., Slemr, F., and Conrad, R.: Microbial production and uptake of nitric oxide in soil, FEMS Microbiol. Ecol., 62, 221–230, https://doi.org/10.1111/j.1574-6968.1989.tb03696.x, 1989.

Scharko, N. K., Schütte, U. M. E., Berke, A. E., Banina, L., Peel, H. R., Donaldson, M. A., Hemmerich, C., White, J. R., and Raff, J. D.: Combined Flux Chamber and Genomics Approach Links Nitrous Acid Emissions to Ammonia Oxidizing Bacteria and Archaea in Urban and Agricultural Soil, Environ. Sci. Technol., 49, 13825–13834, https://doi.org/10.1021/acs.est.5b00838, 2015.

Sehy, U., Ruser, R., and Munch, J. C.: Nitrous oxide fluxes from maize fields: relationship to yield, site-specific fertilization, and soil conditions, Agr. Ecosyst. Environ., 99, 97–111, https://doi.org/10.1016/s0167-8809(03)00139-7, 2003.

Skiba, U., Smith, K. A., and Fowler, D.: Nitrification and denitrification as sources of nitric oxide and nitrous oxide in a sandy loam soil, Soil Biol. Biochem., 25, 1527–1536, https://doi.org/10.1016/0038-0717(93)90007-X, 1993.

Song, Y., Zhang, Y., Xue, C., Liu, P., He, X., Li, X., and Mu, Y.: The seasonal variations and potential sources of nitrous acid (HONO) in the rural North China Plain, Environ. Pollut., 311, 119967, https://doi.org/10.1016/j.envpol.2022.119967, 2022.

Song, Y., Xue, C., Zhang, Y., Liu, P., Bao, F., Li, X., and Mu, Y.: Measurement report: Exchange fluxes of HONO over agricultural fields in the North China Plain, Atmos. Chem. Phys., 23, 15733–15747, https://doi.org/10.5194/acp-23-15733-2023, 2023.

Sörgel, M., Regelin, E., Bozem, H., Diesch, J.-M., Drewnick, F., Fischer, H., Harder, H., Held, A., Hosaynali-Beygi, Z., Martinez, M., and Zetzsch, C.: Quantification of the unknown HONO daytime source and its relation to NO_2, Atmos. Chem. Phys., 11, 10433–10447, https://doi.org/10.5194/acp-11-10433-2011, 2011.

Sörgel, M., Trebs, I., Wu, D., and Held, A.: A comparison of measured HONO uptake and release with calculated source strengths in a heterogeneous forest environment, Atmos. Chem. Phys., 15, 9237–9251, https://doi.org/10.5194/acp-15-9237-2015, 2015.

Stella, P., Loubet, B., Laville, P., Lamaud, E., Cazaunau, M., Laufs, S., Bernard, F., Grosselin, B., Mascher, N., Kurtenbach, R., Mellouki, A., Kleffmann, J., and Cellier, P.: Comparison of methods for the determination of NO-O_3-NO_2 fluxes and chemical interactions over a bare soil, Atmos. Meas. Tech., 5, 1241–1257, https://doi.org/10.5194/amt-5-1241-2012, 2012.

Stemmler, K., Ammann, M., Donders, C., Kleffmann, J., and George, C.: Photosensitized reduction of nitrogen dioxide on humic acid as a source of nitrous acid, Nature, 440, 195–198, https://doi.org/10.1038/nature04603, 2006.

Su, H., Cheng, Y. F., Cheng, P., Zhang, Y. H., Dong, S., Zeng, L. M., Wang, X., Slanina, J., Shao, M., and Wiedensohler, A.: Observation of nighttime nitrous acid (HONO) formation at a non-urban site during PRIDE-PRD2004 in China, Atmos. Environ., 42, 6219–6232, https://doi.org/10.1016/j.atmosenv.2008.04.006, 2008.

Su, H., Cheng, Y., Oswald, R., Behrendt, T., Trebs, I., Meixner, F. X., Andreae, M. O., Cheng, P., Zhang, Y., and Pöschl, U.: Soil nitrite as a source of atmospheric HONO and OH radicals, Science, 333, 1616–1618, https://doi.org/10.1126/science.1207687, 2011.

Sutton, M. A., Fowler, D., and Moncrieff, J. B.: The exchange of atmospheric ammonia with vegetated surfaces. I: Unfertilized vegetation, Q. J. Roy. Meteor. Soc., 119, 1023–1045, https://doi.org/10.1016/S1352-2310(97)00164-7, 1993.

Tang, K., Qin, M., Duan, J., Fang, W., Meng, F., Liang, S., Xie, P., Liu, J., Liu, W., Xue, C., and Mu, Y.: A dual dynamic chamber system based on IBBCEAS for measuring fluxes of nitrous acid in agricultural fields

in the North China Plain, Atmos. Environ., 196, 10–19, https://doi.org/10.1016/j.atmosenv.2018.09.059, 2019.

Tang, K., Qin, M., Fang, W., Duan, J., Meng, F., Ye, K., Zhang, H., Xie, P., Liu, J., Liu, W., Feng, Y., Huang, Y., and Ni, T.: An automated dynamic chamber system for exchange flux measurement of reactive nitrogen oxides (HONO and NO_x) in farmland ecosystems of the Huaihe River Basin, China, Sci. Total Environ., 745, 140867, https://doi.org/10.1016/j.scitotenv.2020.140867, 2020.

Tang, Y., An, J., Wang, F., Li, Y., Qu, Y., Chen, Y., and Lin, J.: Impacts of an unknown daytime HONO source on the mixing ratio and budget of HONO, and hydroxyl, hydroperoxyl, and organic peroxy radicals, in the coastal regions of China, Atmos. Chem. Phys., 15, 9381–9398, https://doi.org/10.5194/acp-15-9381-2015, 2015.

Vandenboer, T. C., Brown, S. S., Murphy, J. G., Keene, W. C., Young, C. J., Pszenny, A. A. P., Kim, S., Warneke, C., De Gouw, J. A., Maben, J. R., Wagner, N. L., Riedel, T. P., Thornton, J. A., Wolfe, D. E., Dubé, W. P., Öztürk, F., Brock, C. A., Grossberg, N., Lefer, B., Lerner, B., Middlebrook, A. M., and Roberts, J. M.: Understanding the role of the ground surface in HONO vertical structure: High resolution vertical profiles during NACHTT-11, J. Geophys. Res.-Atmos., 118, 10155–10171, https://doi.org/10.1002/jgrd.50721, 2013.

VandenBoer, T. C., Markovic, M. Z., Sanders, J. E., Ren, X., Pusede, S. E., Browne, E. C., Cohen, R. C., Zhang, L., Thomas, J., Brune, W. H., and Murphy, J. G.: Evidence for a nitrous acid (HONO) reservoir at the ground surface in Bakersfield, CA, during CalNex 2010, J. Geophy. Res., 119, 9093–9106, https://doi.org/10.1002/2013JD020971, 2014.

Vandenboer, T. C., Young, C. J., Talukdar, R. K., Markovic, M. Z., Brown, S. S., Roberts, J. M., and Murphy, J. G.: Nocturnal loss and daytime source of nitrous acid through reactive uptake and displacement, Nat. Geosci., 8, 55–60, https://doi.org/10.1038/ngeo2298, 2015.

von der Heyden, L., Wißdorf, W., Kurtenbach, R., and Kleffmann, J.: A relaxed eddy accumulation (REA) LOPAP system for flux measurements of nitrous acid (HONO), Atmos. Meas. Tech., 15, 1983–2000, https://doi.org/10.5194/amt-15-1983-2022, 2022.

Wang, Y., Fu, X., Wu, D., Wang, M., Lu, K., Mu, Y., Liu, Z., Zhang, Y., and Wang, T.: Agricultural Fertilization Aggravates Air Pollution by Stimulating Soil Nitrous Acid Emissions at High Soil Moisture, Environ. Sci. Technol., 55, 14556–14566, https://doi.org/10.1021/acs.est.1c04134, 2021.

Weber, B., Wu, D., Tamm, A., Ruckteschler, N., Rodríguez-Caballero, E., Steinkamp, J., Meusel, H., Elbert, W., Behrendt, T., Sörgel, M., Cheng, Y., Crutzen, P. J., Su, H., Pöschl, U., and Wofsy, S. C.: Biological soil crusts accelerate the nitrogen cycle through large NO and HONO emissions in drylands, P. Natl. Acad. Sci. USA, 112, 15384–15389, https://doi.org/10.1073/pnas.1515818112, 2015.

Wong, K. W., Tsai, C., Lefer, B., Grossberg, N., and Stutz, J.: Modeling of daytime HONO vertical gradients during SHARP 2009, Atmos. Chem. Phys., 13, 3587–3601, https://doi.org/10.5194/acp-13-3587-2013, 2013.

Wu, D., Kampf, C. J., Pöschl, U., Oswald, R., Cui, J., Ermel, M., Hu, C., Trebs, I., and Sörgel, M.: Novel tracer method to measure isotopic labeled gas-phase nitrous acid ($HO^{15}NO$) in biogeochemical studies, Environ. Sci. Technol., 48, 8021–8027, https://doi.org/10.1021/es501353x, 2014.

Wu, D., Horn, M. A., Behrendt, T., Müller, S., Li, J., Cole, J. A., Xie, B., Ju, X., Li, G., Ermel, M., Oswald, R., Fröhlich-Nowoisky, J., Hoor, P., Hu, C., Liu, M., Andreae, M. O., Pöschl, U., Cheng, Y., Su, H., Trebs, I., Weber, B., and Sörgel, M.: Soil HONO emissions at high moisture content are driven by microbial nitrate reduction to nitrite: tackling the HONO puzzle, ISME J., 13, 1688–1699, https://doi.org/10.1038/s41396-019-0379-y, 2019.

Wu, D., Zhang, J., Wang, M., An, J., Wang, R., Haider, H., Huang, Y., Zhang, Q., Zhou, F., Tian, H., Zhang, X., Deng, L., Pan, Y., Chen, X., Yu, Y., Hu, C., Wang, R., Song, Y., Gao, Z., Wang, Y., Hou, L., and Liu, M.: Global and Regional Patterns of Soil Nitrous Acid Emissions and Their Acceleration of Rural Photochemical Reactions, J. Geophys. Res.-Atmos., 127, e2021JD036379, https://doi.org/10.1029/2021JD036379, 2022.

Xu, W., Kuang, Y., Zhao, C., Tao, J., Zhao, G., Bian, Y., Yang, W., Yu, Y., Shen, C., Liang, L., Zhang, G., Lin, W., and Xu, X.: NH_3-promoted hydrolysis of NO_2 induces explosive growth in HONO, Atmos. Chem. Phys., 19, 10557–10570, https://doi.org/10.5194/acp-19-10557-2019, 2019.

Xue, C., Ye, C., Zhang, Y., Ma, Z., Liu, P., Zhang, C., Zhao, X., Liu, J., and Mu, Y.: Development and application of a twin open-top chambers method to measure soil HONO emission in the North China Plain, Sci. Total Environ., 659, 621–631, https://doi.org/10.1016/j.scitotenv.2018.12.245, 2019.

Xue, C., Zhang, C., Ye, C., Liu, P., Catoire, V., Krysztofiak, G., Chen, H., Ren, Y., Zhao, X., Wang, J., Zhang, F., Zhang, C., Zhang, J., An, J., Wang, T., Chen, J., Kleffmann, J., Mellouki, A., and Mu, Y.: HONO budget and its role in nitrate formation in the rural North China Plain, Environ. Sci. Technol., 54, 11048–11057, https://doi.org/10.1021/acs.est.0c01832, 2020.

Xue, C., Ye, C., Kleffmann, J., Zhang, W., He, X., Liu, P., Zhang, C., Zhao, X., Liu, C., Ma, Z., Liu, J., Wang, J., Lu, K., Catoire, V., Mellouki, A., and Mu, Y.: Atmospheric measurements at Mt. Tai – Part II: HONO budget and radical ($RO_x + NO_3$) chemistry in the lower boundary layer, Atmos. Chem. Phys., 22, 1035–1057, https://doi.org/10.5194/acp-22-1035-2022, 2022.

Xue, C., Ye, C., Lu, K., Liu, P., Zhang, C., Su, H., Bao, F., Cheng, Y., Wang, W., Liu, Y., Catoire, V., Ma, Z., Zhao, X., Song, Y., Ma, X., McGillen, M. R., Mellouki, A., Mu, Y., and Zhang, Y.: Reducing Soil-Emitted Nitrous Acid as a Feasible Strategy for Tackling Ozone Pollution, Environ. Sci. Technol., 58, 9227–9235, https://doi.org/10.1021/acs.est.4c01070, 2024.

Yamulki, S. and Jarvis, S. C.: Short-term effects of tillage and compaction on nitrous oxide, nitric oxide, nitrogen dioxide, methane and carbon dioxide fluxes from grassland, Biol. Fert. Soils, 36, 224–231, https://doi.org/10.1007/s00374-002-0530-0, 2002.

Yao, Z., Zheng, X., Xie, B., Mei, B., Wang, R., Butterbach-Bahl, K., Zhu, J., and Yin, R.: Tillage and crop residue management significantly affects N-trace gas emissions during the non-rice season of a subtropical rice-wheat rotation, Soil Biol. Biochem., 41, 2131–2140, https://doi.org/10.1016/j.soilbio.2009.07.025, 2009.

Ye, C., Zhang, N., Gao, H., and Zhou, X.: Photolysis of Particulate Nitrate as a Source of HONO and NO_x, Environ. Sci. Technol., 51, 6849–6856, https://doi.org/10.1021/acs.est.7b00387, 2017.

Ye, C., Lu, K., Ma, X., Qiu, W., Li, S., Yang, X., Xue, C., Zhai, T., Liu, Y., Li, X., Li, Y., Wang, H., Tan, Z., Chen, X., Dong, H., Zeng, L., Hu, M., and Zhang, Y.: HONO chemistry at a subur-

ban site during the EXPLORE-YRD campaign in 2018: formation mechanisms and impacts on O_3 production, Atmos. Chem. Phys., 23, 15455–15472, https://doi.org/10.5194/acp-23-15455-2023, 2023.

Zhang, N., Zhou, X., Bertman, S., Tang, D., Alaghmand, M., Shepson, P. B., and Carroll, M. A.: Measurements of ambient HONO concentrations and vertical HONO flux above a northern Michigan forest canopy, Atmos. Chem. Phys., 12, 8285–8296, https://doi.org/10.5194/acp-12-8285-2012, 2012.

Zhang, X., Davidson, E. A., Mauzerall, D. L., Searchinger, T. D., Dumas, P., and Shen, Y.: Managing nitrogen for sustainable development, Nature, 528, 51–59, https://doi.org/10.1038/nature15743, 2015.

Zhou, X., Gao, H., He, Y., Huang, G., Bertman, S. B., Civerolo, K., and Schwab, J.: Nitric acid photolysis on surfaces in low-NO_x environments: Significant atmospheric implications, Geophys. Res. Lett., 30, 2217, https://doi.org/10.1029/2003GL018620, 2003.

Zhou, X., Zhang, N., Teravest, M., Tang, D., Hou, J., Bertman, S., Alaghmand, M., Shepson, P. B., Carroll, M. A., Griffith, S., Dusanter, S., and Stevens, P. S.: Nitric acid photolysis on forest canopy surface as a source for tropospheric nitrous acid, Nat. Geosci., 4, 440–443, https://doi.org/10.1038/ngeo1164, 2011.